

## The effect of emergent vegetation on convective flushing in shallow wetlands: Scaling and experiments

C. E. Oldham<sup>1</sup>

Centre for Water Research, University of Western Australia, Nedlands, Western Australia 6907, Australia

J. J. Sturman

Remote Area Developments Group, Environmental Science, Murdoch University, Murdoch, Western Australia 6015, Australia

### Abstract

Many wetlands around the world are characterized by shallow water, dense vegetation in the littoral zones, no significant riverine inflow and minimal circulation. Recent research on the hydrodynamics of such wetlands has identified convective circulation as being important for flushing of the littoral zones. To quantify this process, a parameterization of the convective discharge per unit width, which had been previously developed for nonvegetated systems, was extended to include a drag coefficient dependent on Reynolds number and vegetation density. The drag coefficient also included the effect of anisotropic permeability of the vegetation. The effects of relatively dense emergent vegetation (~17% by volume) on convective flushing of shallow wetlands with low-Reynolds number (~100) flow was then investigated using experiments in a laboratory convection tank (0.5 by 2 by 0.1 m) and in a wetland mesocosm (5 by 15 by 1 m). Bottom convective currents of ~1–10 mm s<sup>-1</sup> were measured in both the laboratory and the mesocosm. These currents resulted in the shallow, vegetated regions of the mesocosm being flushed in 4 h. The discharge per unit width (m<sup>2</sup> s<sup>-1</sup>) predicted by the developed parameterization compared favorably ( $R^2 = 0.7$ ) with the discharge per unit width measured in both the laboratory and the mesocosm. The short timescales of convective flushing, even in the presence of reasonably dense vegetation, indicate the likely significance of this mechanism in sheltered wetlands.

Convective circulation occurs in aquatic systems when shallow waters heat or cool more rapidly than deeper waters, causing horizontal gradients in water temperature and density. The horizontal density differences drive convective currents, which allow increased flushing of the littoral regions. In wetlands, these littoral zones are typically characterized by dense emergent vegetation, yet the effect of vegetation on convective circulation has rarely been addressed. This paper develops parameterizations to describe that effect, then presents some preliminary laboratory and field data to test the parameterization.

Convective currents have been frequently observed in deep lakes (e.g., Monismith et al. 1990; Nepf and Oldham 1997), and they have also been measured in shallow wetlands. Arnold and Oldham (1997) measured the distinctive signals of cool convective currents inserting along the bottom boundary of a shallow (2 m deep) wetland (Fig. 1) for >30% of the year. These bottom currents are typically 0 (1–10) mm s<sup>-1</sup> (Sturman et al. 1999). Although this is low compared to currents measured in lakes dominated by river in-

flows, in lentic systems such as groundwater-fed wetlands, these currents may be significant for wetland ecology.

Convective flushing timescales in wetlands have previously been quantified by Sturman et al. (1999), who adapted scaling arguments from convective dynamics on geophysical scales (Sturman and Ivey 1998). However, the work of Sturman et al. (1999) did not take into account the effect of emergent vegetation on the convective flushing characteristics. Horsch and Stefan (1988) presented a preliminary model of convective circulation through emergent vegetation; however, their assumptions regarding the nature of drag imply that the vegetation density decreased linearly with depth. That model has not, to our knowledge, been tested experimentally.

Although we focus in this paper specifically on convective circulation through emergent vegetation, there has been increasing interest recently in the general question of how vegetation affects hydrodynamics. In most cases, the effect of emergent vegetation has been incorporated into a bulk drag coefficient, whether based on a single cylinder or arrays of emergent vegetation (Nepf and Koch 1999). Nepf (1999) presented a model for the estimation of diffusion and drag in flows with Reynolds number  $> \approx 200$ , a regime in which the drag coefficient is only a weak function of Re. Indeed most experimental work on the effect of vegetation on hydrodynamics has been done on high-Reynolds number flow (e.g., Escartin and Aubrey 1995; Nepf and Koch 1999). Such high-Reynolds number flows are expected in lakes dominated by river inflows or in shallow tidal embayments. In contrast, convective circulation in lentic wetlands creates flows through vegetation with Reynolds number ~0(100)

<sup>1</sup> Corresponding author (oldham@cwr.uwa.edu.au).

### Acknowledgments

We thank Iain Rea for collecting the laboratory and mesocosm data; Greg Ivey for allowing us access to his convection tank; Greg Ivey, David Luketina, Mike Coates, and Jose Romero for useful comments on the original manuscript; and Mark Lund and Paul Lavery at Edith Cowan University for allowing us access to their wetland mesocosms. J.J.S. was supported by the Australian Research Council. Centre for Water Research report ED1459JS.

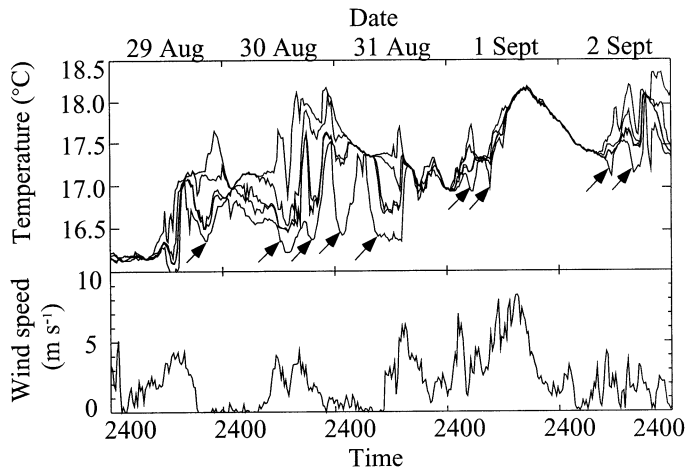


Fig. 1. Thermistor chain and wind speed data collected in Lake Yangebup in Western Australia, over 5 d. The five thermistors were suspended at 0.4-m intervals from the surface. The arrows indicate convective bottom current signals in the thermistor chain data (i.e., rapid cooling of bottom waters without concurrent cooling of surface waters). Figure taken from Arnold and Oldham 1997.

and therefore falls outside the conditions parameterized by Nepf (1999). In order to conceptualize the effects of vegetation on flow in these environments, we used parameterizations developed for porous media flow. We were therefore able to use existing values for drag coefficients taken from porous media flow literature (Eckert and Drake 1972, for Reynolds number  $>100$ ; Lee and Yang 1997, for  $1 < \text{Reynolds number} < 50$ ).

The overall aim of the work presented here was to extend the convective circulation scaling used by Sturman et al. (1999) to account for emergent vegetation using porous media flow parameterization of drag coefficients. We then conducted simple laboratory experiments and preliminary field experiments to test the developed scaling and the Horsch and Stefan (1988) model. In our comparison of the models, and also in our laboratory and field experiments, we focus on determining the timescales of flushing of the shallow regions.

### Scaling analysis

To compare the discharge per unit width (also known as the 2D discharge) and flushing timescales across experiments in the laboratory and the field, we developed scaling arguments to describe the convective dynamics. Such scaling effectively normalizes our experimental results to variables such as buoyancy flux, dimensions of the water body, or the spacing : diameter ratio of the vegetation. Scaling also allows us to apply hypotheses regarding the forcing of convective circulation to other studies, whether in the laboratory or the field, where conditions may be very different.

Sturman et al. (1999) developed scaling relationships to describe convective currents in nonvegetated wetlands. In the following section, we extend the scaling of Sturman et al. (1999) to include the effect of vegetation. A summary of the scaling derivation is presented below; however, readers

Table 1. Summary of variables used in the text.

Variable	Description	Units
$\overline{w'T'}$	Mean vertical turbulent heat flux	$^{\circ}\text{C m s}^{-1}$
$B$	Buoyancy flux	$\text{m}^2 \text{s}^{-3}$
$c$	Forchheimer coefficient	dimensionless
$d$	Vegetation diameter	m
$F_r$	Added resistance to flow caused by convection-induced boundary layer	$\text{N m}^{-3}$
$g$	Gravitational acceleration	$\text{m s}^{-2}$
$h$	Thickness of the geometrically unconstrained turbulent boundary layer	m
$h_g$	Thickness of the gravity current or underflow	m
$H$	Depth of water body at end of slope region	m
$k_x$	Permeability of vegetated region in $x$ direction	$\text{m}^2$
$k_z$	Permeability of vegetated region in $z$ direction	$\text{m}^2$
$\ell$	Length of convective forcing region above slope	m
$\ell_1$	Horizontal length scale over which the turbulent boundary layer is not geometrically constrained by underflow	m
$p$	Pressure drop across vegetation	$\text{N m}^{-2}$
$Q$	2D discharge	$\text{m}^2 \text{s}^{-1}$
$Q_{\text{EX}}$	Measured 2D discharge	$\text{m}^2 \text{s}^{-1}$
$Q_{\text{HS}}$	Estimated 2D discharge using scaling of Horsch and Stefan (1988)	$\text{m}^2 \text{s}^{-1}$
$Q_{\text{NOVEG}}$	Estimated 2D discharge using scaling of Sturman et al. (1998)	$\text{m}^2 \text{s}^{-1}$
$Ra$	Rayleigh number	dimensionless
$Re$	Reynolds number	dimensionless
$s$	Vegetation spacing, center-to-center	m
$T'$	Temperature fluctuation	$^{\circ}\text{C}$
$u$	Horizontal velocity	$\text{m s}^{-1}$
$w'$	Vertical velocity fluctuation	$\text{m s}^{-1}$
$T$	Temperature	$^{\circ}\text{C}$
$\alpha$	Coefficient of thermal expansion	$\text{K}^{-1}$
$\mu$	Dynamic viscosity	$\text{N s m}^{-2}$
$\theta$	Slope of vegetated region	radians
$\rho$	Density of water	$\text{kg m}^{-3}$
$\tau$	Flushing timescale of vegetated sloping region	s

interested only in the applications of these equations should pass directly to Eqs. 9 and 10 and then to the experimental section. These equations show how the 2D discharge and flushing timescales are functions of the buoyancy flux, the length of the sloping region, the angle of the slope, and coefficients relating to the vegetation density. Note that a summary of all notation used is given in Table 1.

*Detailed scaling derivations*—Conceptually, we consider the wetland to be two back-to-back wedges, whereas the emergent vegetation will be modeled as staggered rows of vertical tubes exposed to a cross flow (Fig. 2C). Cooling at the water surface gives rise to thermals, which plunge down between the tubes (vegetation). A key concept in this model is that there is much greater permeability to flow in the  $z$

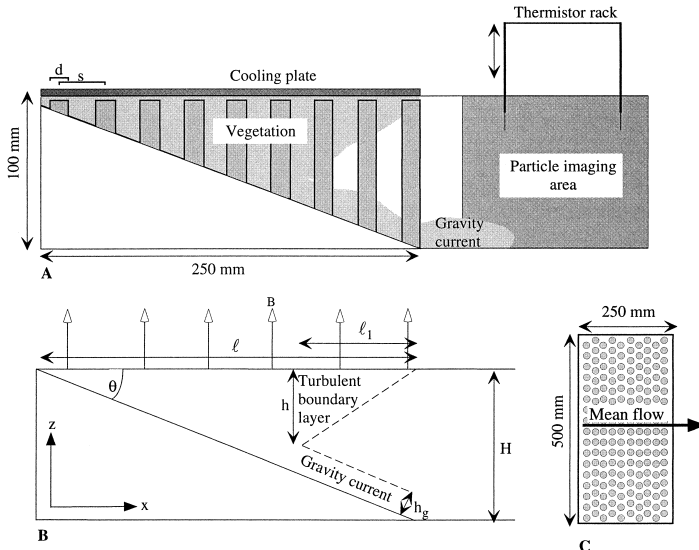


Fig. 2. (A) Schematic of the laboratory apparatus dimensions, (B) the length scales used in the parameterization of 2D discharge, and (C) an areal view of the staggered array of PVC cylinders, with the bold arrow indicating undercurrent direction.

direction compared to the  $x$  direction. In our laboratory experiments described below, we found that the permeability in the  $z$  direction was about 1,000 times greater than the permeability in the  $x$  direction.

Another key concept is that the flow of cooler water down the sloping region, defined within the underflow thickness  $h_g$  (Fig. 2B), is the same as the rate at which eddies form at the water surface, scaled over the horizontal length  $\ell_1$  (Fig. 2B). By conservation of mass, these two discharges must be equal.

### Momentum equations

We consider both the horizontal and the vertical components of the momentum equation. The horizontal momentum equation can be modeled as a generalization of the D'arcy Forchheimer equation for porous media flow (Knupp and Lage 1995).

$$\frac{\partial p}{\partial x} = \frac{\mu u}{k_x} + \frac{c \rho u^2}{k_x^{1/2}} \left( \frac{k_z}{k_x} \right)^{1/3} + F_r, \quad (1)$$

$p$  is the pressure drop through the porous medium ( $\text{N m}^{-2}$ ),  $x$  is the horizontal coordinate of the medium ( $\text{m}$ ),  $\mu$  is the dynamic viscosity ( $\text{N s m}^{-2}$ ),  $u$  is the macroscopic horizontal velocity ( $\text{m s}^{-1}$ ),  $k_x$  is the permeability of the porous medium in the  $x$  direction ( $\text{m}^2$ ),  $k_z$  is the permeability of the porous medium in the vertical direction ( $\text{m}^2$ ),  $\rho$  is the fluid density ( $\text{kg m}^{-3}$ ),  $c$  is the Forchheimer coefficient, and  $F_r$  is the added resistance to the flow due to the boundary layer associated with the forcing flux through the surface ( $\text{N m}^{-2}$ ). The term

$$\frac{c}{k_x^{1/2}} \left( \frac{k_z}{k_x} \right)^{1/3}$$

is a form of inertial drag coefficient for flow across the cylinders or vegetation (Ward 1964). Also note that Knupp and Lage (1995) only included the first two terms on the right-hand side, and we have added the final term for completeness.

For convective circulation in the presence of a moderate density of vegetation, Eq. 1 can be rewritten as an inertia-pressure balance.

$$0 \sim -\frac{1}{\rho} \frac{\partial p}{\partial x} + \frac{c u^2}{k_x^{1/2}} \left( \frac{k_z}{k_x} \right)^{1/3} \quad (2)$$

In the vertical direction, the dominant balance in the momentum equation can be expressed as

$$0 \sim \frac{1}{\rho} \frac{\partial p}{\partial z} + g \alpha \Delta T, \quad (3)$$

where  $\alpha$  ( $\text{K}^{-1}$ ) is the coefficient of thermal expansion and  $g$  ( $\text{m s}^{-2}$ ) is the acceleration due to gravity.

### Thermal energy equation

The thermal energy equation provides the other relationship necessary to obtain a solution. If we assume that the vertical turbulent diffusion of heat into the fluid is balanced by mean horizontal convection, then the thermal energy equation reduces to

$$u \frac{\partial T}{\partial x} \sim \frac{\partial (\overline{w'T'})}{\partial z}, \quad (4)$$

where  $w'$  is the vertical velocity fluctuation,  $T'$  is the temperature fluctuation and  $\overline{w'T'}$  is the mean vertical turbulent heat flux.

Like Sturman et al. (1996), we introduce into Eq. 4 the scales  $x \sim \ell_1$  and  $z \sim h$ , where  $\ell_1$  is the length of the forcing region above the unconstrained boundary layer and  $h$  is the unknown thickness of the boundary layer (Fig. 2). We also introduce into Eq. 4  $\Delta T \sim B^{2/3}/g\alpha z^{1/3}$  (Chou et al. 1986) and  $\overline{w'T'} \sim B/\alpha g$ , where  $B$  ( $\text{m}^2 \text{s}^{-3}$ ) is the buoyancy flux at the water surface. The outcome of substituting the scales from above into Eq. 4 is

$$u \sim B^{1/3} \ell_1 / h^{2/3}. \quad (5)$$

The scaling of Chou et al. (1986) was derived from measurements in high-Reynolds number flows, but this scaling has been successfully applied to a low-Reynolds number situation (Sturman et al. 1996). Thus, we believe Chou et al.'s (1986) scaling to be appropriate here when the vegetation is reasonably widely spaced and the inertia-pressure balance of the momentum equation holds.

### 2D discharge and flushing timescales

In order to determine  $u$  and  $h$  from the initial variables, the momentum equation must be cross-differentiated, and after eliminating pressure we find that

$$\frac{\partial}{\partial z} \left( \frac{c \rho u^2}{k_x^{1/2}} \right) \left( \frac{k_z}{k_x} \right)^{1/3} \sim \frac{\partial}{\partial x} (\rho g \alpha \Delta T) \quad (6)$$

Substituting the scales  $\Delta T \sim B^{2/3}/g\alpha z^{1/3}$  (Chou et al. 1986) together with  $x \sim \ell_1$  and  $z \sim h$  and using Eq. 5, we obtain the following two equations.

$$u \sim \left[ \frac{Bk_x^{1/2}}{c} \left( \frac{k_x}{k_z} \right)^{1/3} \right]^{1/3} \quad (7)$$

$$h \sim \left[ \ell_1^3 \frac{c}{k_x^{1/2}} \left( \frac{k_z}{k_x} \right)^{1/3} \right]^{1/2} \quad (8)$$

If  $h_g$  is small, then  $h \sim (\ell - \ell_1)\tan \theta$ , and when  $\theta$  is small,  $\ell_1/\ell$  is also small. Therefore the two-dimensional discharge from the boundary layer, estimated by  $Q \sim uh$ , is given as

$$Q \sim \left[ B \frac{k_x^{1/2}}{c} \left( \frac{k_x}{k_z} \right)^{1/3} \right]^{1/3} \ell \tan \theta. \quad (9)$$

By conservation of mass, this 2D discharge equals the discharge of the undercurrent, which is one of the two major variables we sought to derive in this study. The coefficients  $c$ ,  $k_x$  and  $k_z$  are determined empirically, as described below.

The other major variable, the flushing timescale, is the time taken for the water in the wedge region to be exchanged completely, and it is given by the wedge volume divided by the 2D discharge. In wetlands modeled by back-to-back wedges, this timescale is given by

$$\tau \sim \ell H/2Q \sim \ell H/Q. \quad (10)$$

### Determination of coefficients $c$ and $k$

In general terms, the empirical coefficients  $c$  and  $k$  are functions of the morphology of the tube array, its orientation to the flow, and the Reynolds number of the flow. Vertical and horizontal Reynolds numbers are determined by

$$\text{Re} = \frac{u_p d}{\nu} \quad (11)$$

where  $u_p$  is the characteristic or ‘‘intertube’’ velocity ( $\text{m s}^{-1}$ ),  $\nu$  is the kinematic viscosity ( $\text{m}^2 \text{s}^{-1}$ ), and  $d$  is the characteristic length scale (m). The intertube velocity is calculated from the downstream velocities and the percentage of volume of vegetation on the slope, assuming conservation of mass.

Calculation of the Reynolds number for flow in the horizontal direction (perpendicular to the vegetation) uses a characteristic length scale,  $d$ , which is simply the cylinder (or vegetation) diameter. Calculation of Reynolds number for flow in the vertical direction (parallel to the vegetation) uses a characteristic length scale, called the hydraulic diameter,  $d_h$ , which is dependent on the spacing : diameter ratio of the vegetation.

$$d_h = d \left( \frac{4(s/d)^2}{\pi} - 1 \right) \quad (12)$$

With the Reynolds numbers, the coefficients  $c$  and  $k$  can now be determined; however, the calculation differs depending on whether the tubes are perpendicular or parallel to the mean flow. The values for  $k$  in both the horizontal and ver-

tical directions give us the permeability ratio  $k_x/k_z$ , known as the flow anisotropy.

For flow parallel to the tubes, or vertical flow, Eckert and Drake (1972, *see* p. 369) defined a pressure drop in terms of a friction factor,  $f_z$ .

$$\frac{\Delta p}{\Delta z} = \frac{f_z \rho u^2}{d_h} \quad (13)$$

Therefore, by equating Eq. 13 with the inertia–pressure term shown in Eq. 2, we find that

$$\frac{c}{k_z^{1/2}} = \frac{f_z}{2d_h}. \quad (14)$$

Given the known values of  $\text{Re}_z$ ,  $f_z$  can be looked up from a Moody diagram in any elementary fluid mechanics text book.

For flow perpendicular to the tubes, or horizontal flow, we use

$$\Delta p = n f_x \rho \frac{u^2}{2} \left( \frac{s}{s-d} \right)^2, \quad (15)$$

where  $n$  is the number of pores in the direction of the flow (Eckert and Drake 1972). Note that Eq. 15 is an adjusted form of the equation, as Eckert and Drake (1972) used pore velocity, rather than the macroscopic velocities required in our derivations.

Comparing Eq. 15 with Eq. 2, we deduce that

$$\frac{c}{k_x^{1/2}} = \frac{f_x}{s\sqrt{3}} \left( \frac{s}{s-d} \right)^2, \quad (16)$$

where the friction factor,  $f_x$ , is obtained from Eckert and Drake (1972, *see* fig. 9-13). Note that the original empirical data of Zhukauskas (1968), from which Eckert and Drake fig. 9-13 was derived, only extends over  $1.25 \leq s/d \leq 2.5$ ; thus, we limit our ability to define  $c/k_x^{1/2}$  to this parameter range. We recall that our laboratory experiments had  $s/d$  ratios of 2.25, and our mesocosm experiments had  $s/d$  ratios of 2. A subset of the Zhukauskas (1968) data, contained within the Eckert and Drake (1972) figures, is presented in Table 2.

Given Eqs. 14 and 16, the ratio of vertical to horizontal permeability to flow can be determined and, therefore, used in Eq. 9.

### Methods

*Laboratory experiments*—The experimental convection cavity comprised a rectangular perspex box of dimensions 2,000 mm long, 500 mm wide, and 100 mm high, with a rigid perspex slope (angle = 22°) inserted into one end (Fig. 2). The tank was insulated with at least 50 mm of polystyrene foam, except for small windows used for flow visualization. A horizontal copper plate (250 mm long by 500 mm wide) was placed along the top of the tank, covering the slope region. Chilled water was circulated behind this plate, causing a destabilizing buoyancy flux into the water from the upper surface of the slope region. Vegetation was modeled by staggered rows of PVC cylinders (12.4 mm outside

Table 2. Values of the friction factor,  $f$  (see Eq. 16), as a function of Reynolds number and porosity, which is characterized by the spacing:diameter ( $s:d$ ) ratio. (Selected data taken from figs. 9–13 in Eckert and Drake 1972.)

$s:d$	Re	$f$
1.25	$10^2$	2.5
	$10^3$	0.8
	$10^4$	0.5
	$10^5$	0.25
1.5	$10^2$	1.5
	$10^3$	0.6
	$10^4$	0.4
	$10^5$	0.2
2.0	$10^2$	1
	$10^3$	0.5
	$10^4$	0.32
	$10^5$	0.17
2.5	$10^2$	0.9
	$10^3$	0.4
	$10^4$	0.26
	$10^5$	0.16

diameter and 15.5 mm apart) inserted along the slope and extending to the water surface (Fig. 2). The spacing (center-center)/diameter ( $s/d$ ) ratio of the cylinders was 2.25 and the areal (and volumetric) density of cylinders along the slope was 17%.

We measured velocities and visualized the flow in the nonslope region by seeding the water with fluorescent particles that ranged in size from 45 to 120  $\mu\text{m}$ . These particles were illuminated close to the tank center by a vertically oriented sheet of laser light from a 4-W argon ion laser. The particle image velocimetry (PIV) method, developed by Stevens and Coates (1994), was used to measure velocities as described in Sturman and Ivey (1998). Temperatures within the nonslope region of the tank were measured by two fast-response thermistors placed 10 and 410 mm from the end of the slope. The thermistors were mounted on a rack driven by a stepper motor, which traversed the 100-mm height of the cavity in 1 s. The thermistors were sampled at 50 Hz, giving a vertical resolution of 2 mm. Temperature profiles were collected every 20 s for the first 5 min of an experiment then approximately every 1 min thereafter. The experiments usually lasted approximately 20 min.

Note that because of the presence of the cylinders (simulating the vegetation) and the cooling plate, neither velocities nor temperatures could be measured in the slope region. These experiments aimed to estimate velocities and flushing timescales of fluid discharged from the slope region, rather than quantify the detailed hydrodynamics surrounding the cylinders.

The inflow and outflow temperatures of the water circulating behind the copper plate were also recorded at the time of each temperature profile. This temperature change, together with the monitored flow rate behind the plate, allowed us to quantify the buoyancy flux across the water surface above the vegetated slope region. An average buoyancy flux was then determined for each experiment.

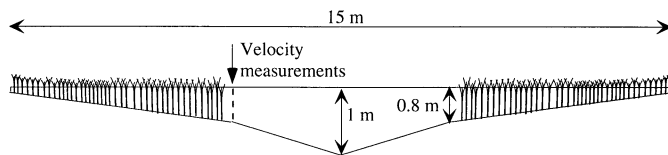


Fig. 3. Schematic of the mesocosm dimensions showing shallow vegetated areas, deeper open water, and typical location of velocity measurements.

*Mesocosm experiments*—The constructed wetland mesocosm used in this experiment was located on the southern outskirts of Perth, Western Australia. The mesocosm was built to the design shown in Fig. 3, was 15 m by 5 m, and contained a combination of shallow and deep regions. The shallow regions promoted vegetation establishment, whereas the deeper regions were too deep for vegetation growth but allowed for particulate settling. In many constructed wetlands, these shallow and deep regions are typically flat bottomed; however, in the mesocosm used for this study, these regions were specifically sloped in order to promote convective circulation. A slope of 1:11 extended for the first 5 m, then changed to a slope of 1:3.5 for the next 2.5 m (Fig. 3). The mesocosm had a minimum depth of 100 mm at both ends and a maximum depth of approximately 1 m at the center.

The mesocosm was vegetated with *Schoenoplectus validus* in the shallow regions (<800 mm deep). This sedge forms tight clumps which, in parallel with our laboratory experiments, we model as circular cylinders. The vegetation clumps had diameters of 0.15 m, a spacing:diameter ratio of approximately 2, and the areal (and volumetric) density of vegetation along the slopes was 16%. It should be noted here that this vegetation density is low for productive wetlands and that treatment wetlands may have greater than 60% plant cover (Kaldec and Knight 1996).

The climate in the region of Perth is Mediterranean, with typical day–night temperature variations of  $\sim 10$ – $15^\circ\text{C}$ . Meteorological conditions were measured by a weather station on site, which combined with surface water temperature, allowed estimation of convective cooling fluxes for the periods of experimental work. Four field trips were undertaken to measure convective currents in the mesocosm; however, on only one were the conditions suitable for convective cooling. A negative heat flux of approximately  $-100 \text{ W m}^{-2}$  was recorded from 1830 h on 21 April until 0800 h the next morning. From 1930 h on 21 April until 0200 h the following morning, there was no wind. This heat flux caused a forcing buoyancy flux of  $3.5 \times 10^{-8} \text{ m}^2 \text{ s}^{-3}$ , which are perfect conditions for the measurement of convective circulation in the mesocosm.

We measured water velocity profiles in the mesocosm using a SONTEK<sup>™</sup> 3D acoustic Doppler velocity (ADV) probe. The probe was mounted on a vertical traversing mechanism, which enabled a vertical velocity profile to be taken in the space of approximately 5 min, sampling at 2 Hz for 30 s at vertical intervals of 100 mm and finishing 100 mm from the sediments. The traversing mechanism was itself mounted on a stiff builders' ladder placed across the

Table 3. Measured and universal parameters.

Experiment	Date (1998)	Water temperature (°C)	$s/d$	Vegetation density (% v/v)	Heat flux ( $\text{W m}^{-2}$ )	Buoyancy flux ( $10^{-6} \text{ m}^2 \text{ s}^{-3}$ )	Underflow velocity ( $\text{mm s}^{-1}$ )	$\ell$ (m)	$\theta$ (deg)	$\nu$ ( $10^{-6} \text{ m}^2 \text{ s}^{-1}$ )	$\alpha$ ( $10^{-4} \text{ K}^{-1}$ )	$Q_{\text{EX}}$ ( $10^{-4} \text{ m}^2 \text{ s}^{-1}$ )
Mesocosm	22 Apr	15	2	16	100	0.035	0.6	5.00	5	1.0	1.5	2.4
Lab 1	11 Jul	19	2.25	17	5,164	2.4	3.1	0.25	22	1.0	1.9	1.0
Lab 2	13 Jul	19	2.25	17	4,949	2.3	4	0.25	22	1.0	1.9	1.4
Lab 3	16 Aug	35	2.25	17	21,627	0.17	6.2	0.25	22	0.8	3.4	2.1
Lab 4	24 Aug (a)	45	2.25	17	26,146	0.26	11.4	0.25	22	0.7	4.2	3.5
Lab 5	24 Aug (b)	35	2.25	17	18,325	0.15	7.3	0.25	22	0.7	3.4	2.1
Lab 6	24 Aug (c)	31.5	2.25	17	11,674	8.7	8	0.25	22	0.6	3.1	3.3

mesocosm. We took ADV profiles at approximately 40-min intervals between 0400 and 1000 h.

## Results

*Laboratory experiments*—The temperature measurements of the water circulating in the cooling plate indicated that the tank was forced with a buoyancy flux averaging  $10^{-5}$ – $10^{-6} \text{ m}^2 \text{ s}^{-3}$  during the six experiments (Table 3).

Velocity vectors derived from the PIV data were calculated every 2.5 mm over the area illuminated by the laser (50 by 140 mm). The velocity vectors measured within the convective undercurrent were then averaged and multiplied by the height of the undercurrent to obtain the two-dimensional discharge,  $Q_{\text{EX}}$  (flow per unit width). An example of a velocity profile extracted from PIV data is shown in Fig. 4. The profile indicates the initial gravity current along the bottom peaking at  $8 \text{ mm s}^{-1}$  and the return flow in the upper water column peaking at  $-3.5 \text{ mm s}^{-1}$ . The gravity current

was around 10 mm thick and was typically  $1.5^\circ\text{C}$  cooler than the overlying water.

The time taken for the cold convective undercurrent to travel from 10 to 410 mm, determined from data collected by the thermistors at these positions, was used as a second estimate of undercurrent velocity. The velocity estimates derived from the thermistor data compared favorably to the velocity estimates derived from PIV data averaged over the area of the cold intrusion ( $R^2 = 0.98$ ).

The two-dimensional discharges, taken as the mean of the PIV and thermistor-derived discharges, ranged from  $1.0 \times 10^{-4}$  to  $3.5 \times 10^{-4} \text{ m}^2 \text{ s}^{-1}$  (Table 3) over the six experiments. These 2D discharges would flush the sloped region of the tank (having a volume of  $0.0125 \text{ m}^3$ ) every 125 s. Conditions within the tank during the six experiments are also shown in Table 3. Note that using the averaged velocities from the PIV and thermistor data, the Reynolds number for vertical flow ranged from 300 to 1,500, and the Reynolds number for horizontal flow ranged from 60 to 300 (Table 4).

*Mesocosm experiments*—Symmetrical convective currents were measured in the mesocosm on the morning on 22 April 1998 (Fig. 5). Surface flows were typically  $1$ – $2 \text{ mm s}^{-1}$ , while bottom undercurrent velocities were around  $0.5 \text{ mm s}^{-1}$ . The symmetrical nature of the velocity profiles is indicative of convectively driven circulation, as opposed to wind-driven circulation. Wind-driven circulation would cause velocity profiles that would have a similar character over the length of the mesocosm (Fig. 6).

Two-dimensional discharges in the mesocosm were estimated by integrating the velocity profiles over the depth of the undercurrent and the return flow. At all times the bottom velocity was assumed to be zero. The 2D discharges, estimated from vertical velocity profiles in the mesocosms, averaged  $2 \times 10^{-4} \text{ m}^2 \text{ s}^{-1}$ . These would result in the wedge of a mesocosm (having a volume of  $15 \text{ m}^3$ ) being flushed in 3.7 h.

The Reynolds number of the vertical flow was 400, and the Reynolds number of the horizontal flow was 100.

## Discussion

Convective circulation may have an effect on temperature stratification and the oxygen budget of wetlands. Field data

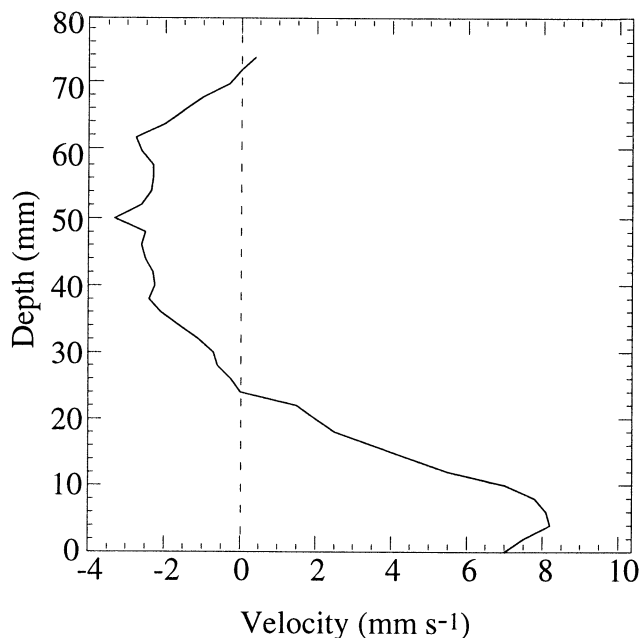


Fig. 4. A convective current velocity profile measured in the laboratory experiment.

Table 4. Calculated parameters.

Experiment	$Re_z$	$Re_x$	Ra ( $10^{10}$ )	$c/k^{1/2}$ ( $m^{-1}$ )	$k_x/k_z$ ( $10^{-4}$ )	$Q$ ( $10^{-4} m^2 s^{-1}$ )	$Q_{HS}$ ( $10^{-4} m^2 s^{-1}$ )	$Q_{NOVEG}$ ( $10^{-4} m^2 s^{-1}$ )	$Q_{EXP}/Q_{NOVEG}$ (%)
Mesocosm	430	100	6.0	7.9	2.3	2.8	8.5	11	26
Lab 1	320	60	1.1	100	2.3	1.1	0.10	5.9	18
Lab 2	400	70	1.1	68	0.28	1.0	0.10	5.8	25
Lab 3	1,000	180	11	48	0.28	2.3	0.13	11	19
Lab 4	1,690	310	18	36	0.11	2.5	0.13	13	27
Lab 5	950	170	9.4	50	0.21	2.0	0.13	11	20
Lab 6	1,230	220	5.0	43	0.15	1.7	0.11	9.0	37

show that the arrival of bottom convective currents in the center of the wetland strengthens the temperature stratification, and laboratory experiments presented above support this. Note however that under these conditions, the water contained within the bottom convective currents has come from the shallow regions and therefore will initially reflect the oxygen content of the shallows. The net diurnal oxygen concentrations in the bottom waters may therefore depend on the comparative timescales of stratification, sediment and water column oxygen demand, biological and physical oxygenation of surface waters, and convective flushing.

The likelihood of convective circulation occurring in a sheltered wetland is dependent on the relative magnitude of convective forcing timescales and the response timescales of the wetland. Typically, convective forcing will occur during nighttime, therefore, with a timescale of  $O(10)$  h. If the wetland response timescale, which we take to be the timescale in which the wetland shallows may be flushed, is of a similar order of magnitude (or less), then convective flushing may occur daily.

These convective flushing timescales have previously

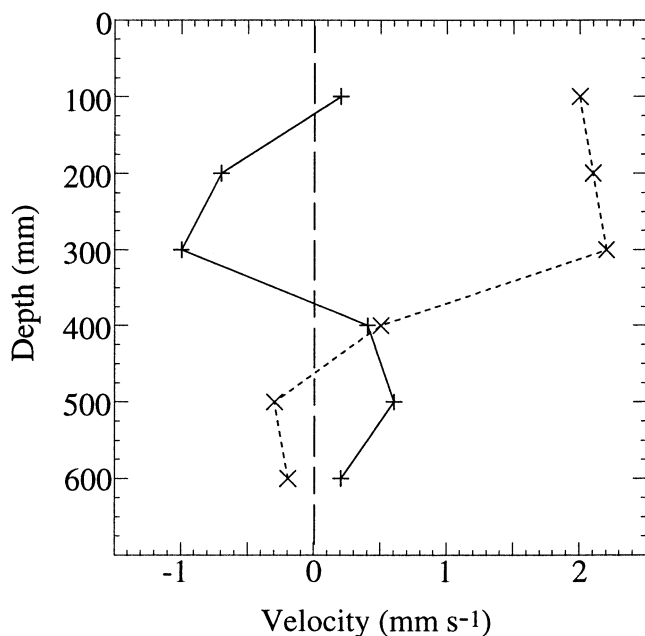


Fig. 5. Convective current velocity profiles measured at different ends of the mesocosm.

been predicted for wetlands with no vegetation. In this paper, we have parameterized these timescales, taking into account vegetation. This work complements research by other workers on flow past vegetation, which has primarily considered high-Reynolds number conditions. In most cases, the effects of vegetation were incorporated into a drag coefficient. The current work uses empirical data from porous media research to define our drag coefficient, which is suitable for flows of Reynolds number  $\sim 100$ . Such low-Reynolds number flows will be prevalent in the densely vegetated wetlands described above. The derived drag coefficient is a function of the Reynolds number of the flow, the density of vegetation, and the anisotropy in the permeability of vegetation to that flow.

The predicted 2D discharges, calculated for each of the experimental conditions, compare favorably ( $R^2 = 0.7$ ) with those measured (Fig. 7). Also, the scaling presented in this paper provides significantly better estimates of the measured discharge than the model presented by Horsch and Stefan (1988) (Fig. 7; Table 4). Horsch and Stefan's model overestimates the discharge in our mesocosms by one order of magnitude and underestimates the discharge in our laboratory experiment by one order of magnitude.

Finally, we compare 2D discharges with and without vegetation. With vegetation at the densities used in our experiments ( $\sim 17\%$  by volume), the discharges were, on average, 20% of those predicted by the scaling of Sturman et al.

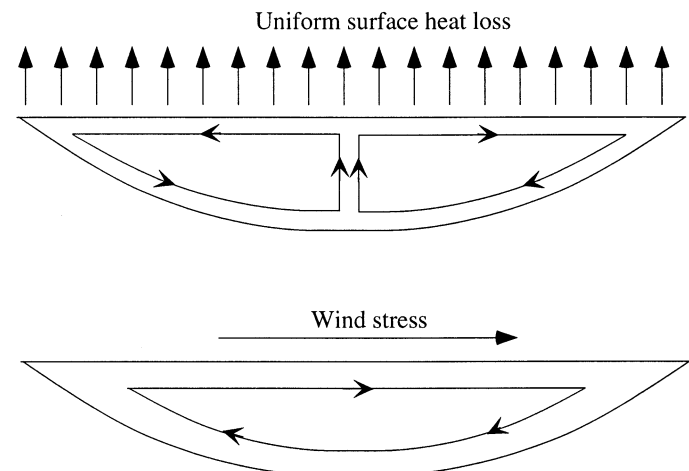


Fig. 6. Schematic of circulation patterns expected during convective forcing (top panel) and wind-driven forcing (bottom panel).

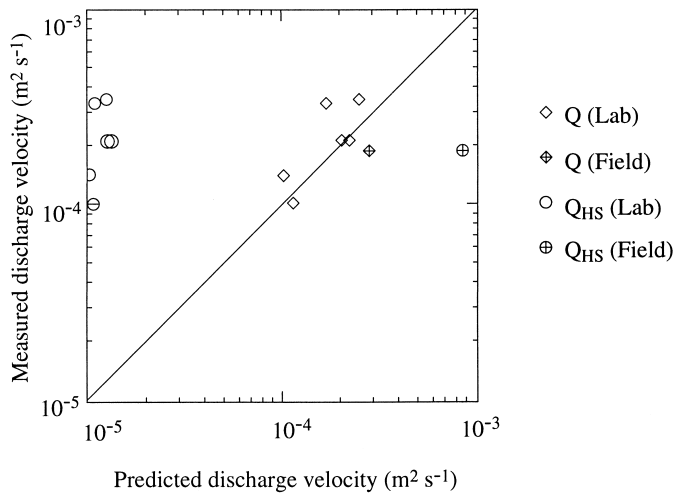


Fig. 7. Comparison of 2D discharges predicted by our scaling with those measured in the laboratory and the mesocosms. Also shown are the 2D discharges predicted by the scaling developed by Horsch and Stefan (1988).

(1999) for flow without vegetation (Table 4). We note that Sturman et al. (1999) showed that the convective discharges measured by James and Barko (1991) in a vegetated wetland was, on average, 20% of those predicted by Sturman et al. (1999). Thus, the new scaling presented above agrees with the field data of James and Barko (1991).

With the decrease in discharge caused by vegetation, the flushing timescales were increased by 80%. Using Eq. 10, we estimated that the vegetated regions of the mesocosms were flushed within  $\sim 4$  h. Our velocity measurements in the mesocosms support this estimate. Without vegetation, the shallows would have been flushed in  $< 1$  h.

This increase in flushing timescales with vegetation has obvious implications for an array of ecological factors, such as particle transport, nutrient uptake, and oxygen budgets. A comparison of such biological timescales, often specific to particular wetland systems, and the transport timescales as estimated by Eq. 10 are now essential to determine the significance of convective circulation in shallow, vegetated, low-flow wetlands.

## References

- ARNOLD, T. N., AND C. E. OLDHAM. 1997. Trace element contamination of a shallow wetland in Western Australia. *Mar. Freshw. Res.* **48**: 531–539.
- CHOU, S.-H., D. ATLAS, AND E.-N. YEH. 1986. Turbulence in a convective marine atmospheric layer. *J. Atmos. Sci.* **43**: 547–564.
- ECKERT, E. R. G., AND R. M. DRAKE. 1972. Analysis of heat and mass transfer. McGraw-Hill.
- ESCARTIN, J., AND D. G. AUBREY. 1995. Flow structure and dispersion within algal mats. *Estuar. Coast. Shelf Sci.* **40**: 451–472.
- HORSCH, G. M., AND H. G. STEFAN. 1988. Convective circulation in littoral water due to surface cooling. *Limnol. Oceanogr.* **33**: 1068–1083.
- JAMES, W. F., AND J. W. BARKO. 1991. Estimation of phosphorus exchange between littoral and pelagic zones during nighttime convective circulation. *Limnol. Oceanogr.* **36**: 179–187.
- KALDEC, R. H., AND R. L. KNIGHT. 1996. Treatment wetlands. Lewis.
- KNUPP, P. M., AND J. L. LAGE. 1995. Generalisation of the Forchheimer-extended Darcy flow model to the tensor permeability case via a variational principle. *J. Fluid Mech.* **299**: 97–104.
- LEE, S. L., AND J. H. YANG. 1997. Modelling of Darcy–Forchheimer drag for fluid flow across a bank of circular cylinders. *Int. J. Heat Mass Transfer* **40**: 3149–3155.
- MONISMITH, S., J. IMBERGER, AND M. L. MORISON. 1990. Convective motions in the sidearm of a small reservoir. *Limnol. Oceanogr.* **35**: 1676–1702.
- NEPF, H. M. 1999. Drag, turbulence and diffusion in flow through emergent vegetation. *Water Resour. Res.* **35**: 479–489.
- NEPF, H. M., AND E. W. KOCH. 1999. Vertical secondary flows in submersed plant-like arrays. *Limnol. Oceanogr.* **44**: 1072–1080.
- NEPF, H. M., AND C. E. OLDHAM. 1997. Exchange dynamics of a shallow contaminated wetland. *Aquatic Sciences* **59**: 193–213.
- STEVENS, C. L., AND M. J. COATES. 1994. A maximised cross-correlation technique for resolving velocity fields in laboratory experiments. *IAHR J. Hydraul. Res.* **32**: 195–211.
- STURMAN, J. J., G. N. IVEY, AND J. R. TAYLOR. 1996. Convection in a long box driven by heating and cooling on the horizontal boundaries. *J. Fluid Mech.* **310**: 61–87.
- STURMAN, J. J., AND G. N. IVEY. 1998. Unsteady convective exchange flows in cavities. *J. Fluid Mech.* **368**: 127–153.
- STURMAN, J. J., C. E. OLDHAM, AND G. N. IVEY. 1999. Steady convective exchange flows down slopes. *Aquat. Sci.* **61**: 260–278.
- WARD, J. C. 1964. Turbulent flow in porous media. *J. Hydraul. Div.: Am. Soc. Chem. Eng.* **90** HY5: 1–12.
- ZHUKAUSKAS, A. A. 1968. Heat transfer in banks of tubes. Mintis, Vilnius, Lithuania.

Received: 7 November 2000

Accepted: 2 April 2001

Amended: 26 April 2001